Improved H_2 Evolution in Quaternary SCIGS Chalcopyrite Semiconductors

Danrui Ni, Hsin-Ya Kuo, James E. Park, Tia S. Lee, Spyder-Rider I. Sloman, Robert J. Cava and Andrew B. Bocarsly**

Department of Chemistry, Princeton University, Princeton, New Jersey 08544, United States

ABSTRACT

In a search for improved photocathode materials for fuel-producing photoelectrochemical cells, quaternary $Ag_xCu_{1-x}Ga_yIn_{1-y}S_2$ ($0 \leqslant x \leqslant 1.0$, $0 \leqslant y \leqslant 1.0$) chalcopyrite semiconductors (SCIGS) were prepared and tested for photochemical hydrogen evolution. The quaternary system, reported here as the first time for bulk materials, enables enhanced control of the materials electronic and electrochemical properties compared to the ternary system. The quaternary system allows for adjustment of the band structures and photocatalytic abilities to a finer degree than is possible in the $Ag_xCu_{1-x}GaS_2$ or $Ag_xCu_{1-x}InS_2$ ternaries, and several of the quaternary $Ag_xCu_{1-x}Ga_yIn_{1-y}S_2$ compositions are found to show better water splitting capability than the ternaries, even when a platinum co-catalyst is present in the ternary systems. Our work on quaternary compounds has led to finding unexpected optoelectric properties in ternary compounds of composition $Ag_xCu_{1-x}GaS_2$. Specifically, a "V-shaped" plot of semiconductor composition versus band gap is observed, which

surprisingly is not easily correlated with the observed variation in semiconductor structure. Even more interesting is the observation that the silver-rich branch of this "V" produces obviously higher H_2 evolution rates than observed with the copper-rich branch.

INTRODUCTION

Photochemical and photoelectrochemical water splitting using semiconductor materials has been widely studied since Honda and Fujishima's 1972 report that n-TiO_2 photoanodes were capable of water oxidation.[1] In the intervening time period, various semiconductor materials have been reported as powdered photocatalysts for water splitting under light irradiation including oxides, oxynitrides, chalcogenides and their solid solutions.[2-6] Visible-light-responsive n-type semiconductor photoanodes have also been prepared to split water.[7-20] Photocathodes based on p-type semiconductors such as $CuRhO_2$ and $AgRhO_2$ have recently been reported,[21,22] however, significantly fewer examples of these materials are known.

Among the candidates for improved water splitting photocathodes, moderate band gap ternary chalcopyrites having a I-III-VI_2 stoichiometry are a promising class of semiconductors for photoelectrochemical water splitting applications. These materials have been studied primarily in a thin film format deposited on cathode surfaces.[23] Many I-III-VI_2 materials have light absorption profiles well-matched to the solar spectrum on the earth, a band gap that straddles the reduction potential of H^+ to H_2 ($E_R^o = 0.00$ V vs. NHE) and the oxidation potential of H_2O to O_2 ($E_R^o = 1.23$ V vs. NHE),[24] and reasonable stability in aqueous electrolytes. Specifically, copper-indium-gallium (CIGS) and silver-indium-gallium (SIGS) chalcogenides are attractive because of their ideal, tunable light-absorption properties and band edge positions.[25] Several studies have

been performed on CIGS- and SIGS-based thin film electrodes investigating their activities in photochemical or photoelectrochemical hydrogen evolution,[24,26,27] as well as application in photovoltaic cells.[28-30]

The ternary CIGS and SIGS systems can be considered the end points of a larger family of quaternary materials in which the ratio of the Group IB metal cations (i.e. Cu and Ag) is varied. Recently, several first-principles DFT studies showed potential for further optimization of photochemical water splitting by CIGS\SIGS quaternary materials through changing the chemical constituents on both the IB and IIIB metal sites.[31,32] These calculations indicated that the band gap values and band edge positions of the CIGS\SIGS quaternaries change when varying the composition of metal sites due to variations in the I-VI and III-VI band interactions, which are primarily responsible for the valence band maximum (VBM) and the conduction band minimum (CBM), respectively. This reveals an approach to shifting both band edge positions and modifying the band structures by changing both the Ag to Cu ratio and the Ga to In ratio, in other words, expanding the currently studied ternary materials to the full family of quaternary "SCIGS" semiconductors. Within this materials' "genome", one can anticipate finding chalcopyrites with suitable band gap and band edge positions that straddle the water redox potentials allowing for efficient photochemical water splitting chemistry. Recently $Ag_xCu_{1-x}Ga_{0.25}In_{0.75}S_2$ thin film electrodes were prepared over a limited compositional range ($0 \leqslant x \leqslant 0.3$),[33] however leaving substantial need for further exploration. This goal motivates the present study of quaternary (Ag,Cu)(Ga,In)S_2 semiconductors having the chalcopyrite crystal structure and a widened compositional range.

For the purposes of this initial investigation, materials were synthesized as powders and evaluated for water reduction under purely photochemical (i.e. not photoelectrochemical) conditions. We find this screen as an efficient methodology for vetting a relatively large number of materials rapidly. And the screen of the (Ag,Cu)(Ga,In)S_2 family revealed that some of the quaternary materials do indeed display photocatalytic properties and stabilities that are superior to the ternaries. The optimal properties are obtained for quaternary compositions near $Ag_{0.75}Cu_{0.25}Ga_{0.25}In_{0.75}S_2$. These materials show photocatalytic hydrogen evolution performance that is comparable to that of ternaries that are noble-metal-loaded.

EXPERIMENTAL METHODS

Preparation of (Ag,Cu)(Ga,In)S_2 Semiconductors. Polycrystalline (Ag,Cu)(Ga,In)S_2 semiconductors were prepared by the solid-state reaction method. Stoichiometric amounts of Cu (Alfa Aesar, 99.999% pure), Ag (Alfa Aesar, 99.999% pure), Ga_2S_3 (Alfa Aesar, 99.999% pure), and In_2S_3 (Alfa Aesar, 99.999% pure) were mixed with elemental sulfur (Alfa Aesar, 99.98%, 5% excess, dried at 120 ºC overnight before use) and sealed in a quartz ampoule after evacuation. The mixture of starting materials was heated at 900–1000 ºC for 72 h. At the end of this time period, the furnace was cooled to room temperature at 3 ºC per hour. No further treatment of the samples was found necessary.

Characterization. The prepared polycrystalline semiconductor powders were characterized by powder X-ray diffraction (XRD) using a Bruker D8 Discover X-ray diffractometer with Cu K_α radiation (λ = 0.15415 nm). Lattice parameters were determined based on least squares fits to the powder XRD patterns by using the Topas diffraction suite. Particle morphology was investigated using an FEI XL30 field-emission gun scanning electron microscope (SEM) equipped with an

Oxford X-Max 20 energy-dispersive X-ray spectroscopy (EDX) running on INCA software. Diffuse reflectance spectra were collected by a Cary 6000i UV-VIS-NIR spectrometer equipped with an integrating sphere and were converted from reflectance to absorbance using the Kubelka-Munk method.[34] The ultraviolet photoelectron spectroscopy (UPS) measurements were performed on a ThermoFisher K-Alpha + X-ray photoelectron spectrometer (XPS/UPS) using the He I (21.2 eV) line.

Photocatalytic Reactions. To achieve high-throughput screening, all photocatalytic reactions were carried out on a homemade light table to ensure concurrent and uniform irradiation. Every photocatalytic hydrogen evolution cell consisted of a 15 mL clear borosilicate glass vial sealed with a polytetrafluoroethylene (PTFE)/silicone septum (Supleco). A weighed amount of photocatalyst powder (ca. 20 mg) was dispersed in 5 mL aqueous solution containing Na_2S (sodium sulfide nanohydrate, $\geqslant$ 98%, 208043 Sigma-Aldrich) and/or Na_2SO_3 as sacrificial electron donors. The photocatalysts were irradiated with 365 nm light from a 3 W light-emitting diode (LED). The light source intensity and vial-to-light-source distance was held constant for all samples using a machined aluminum fixture based on the Bernhard design.[35] Hydrogen product analysis was carried out by gas chromatography. A gas tight syringe was used to withdraw 50 μL of gas from the vial headspace. Samples were analyzed using an SRI 8610C Gas Chromatograph (GC) with a thermal conductivity detector and a Molsieve column (HAYESEP D) with Ar flow gas.

In some cases, the particles were coated with platinum particles as a co-catalyst. To this end, Pt was photo-deposited in-situ from a 8 wt.% concentration of aqueous H_2PtCl_6.[36,37]

RESULTS AND DISCUSSION

Preparation and characterization of $Ag_xCu_{1-x}Ga_yIn_{1-y}S_2$ ($0 \leqslant x \leqslant 1.0$, $0 \leqslant y \leqslant 1.0$).

Figure 1 shows representative powder XRD patterns for the synthesized $Ag_xCu_{1-x}GaS_2$ (x = 0, 0.2, 0.4, 0.6, 0.8 and 1.0) and $Ag_{0.5}Cu_{0.5}Ga_yIn_{1-y}S_2$ (y = 0, 0.25, 0.5, 0.75 and 1.0) chalcopyrites. The XRD patterns of other samples are presented in Figure S1-S5. Compared with the previous preparation of quaternary semiconductor thin films,[33] we have dramatically widened the compositional range of the quaternary system, through both x and y of the bulk semiconductor materials. No secondary phases were observed, indicating the successful formation of quaternary $Ag_xCu_{1-x}Ga_yIn_{1-y}S_2$ solid solutions. The diffraction features can be consistently indexed to a tetragonal unit cell as shown in Figure 1, based on the unit cell structure shown in Figure 2. The diffraction peaks shift systematically with different Ag to Cu and Ga to In ratios, reflecting the variation of lattice parameters due to the differences in ionic radii between Ag^+ (1.00 Å) and Cu^+ (0.60 Å) or Ga^{3+} (0.47 Å) and In^{3+} (0.62 Å).[27]

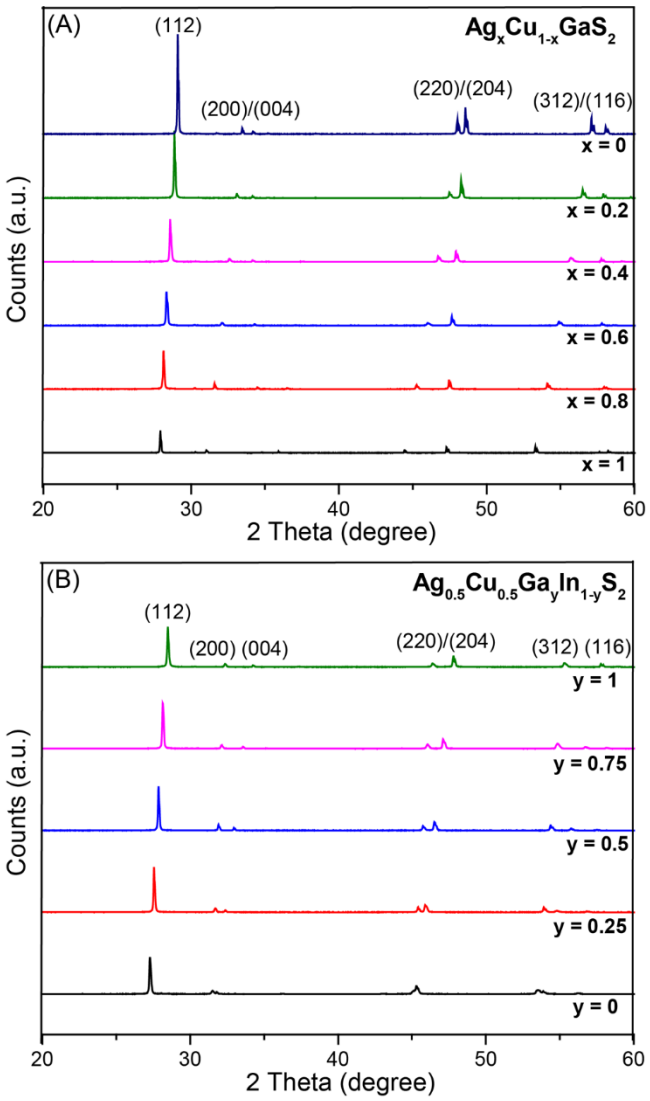

Figure 1. Representative powder X-ray diffraction patterns of (A) $Ag_xCu_{1-x}GaS_2$ for x = 0, 0.2, 0.4, 0.6, 0.8, and 1, and (B) $Ag_{0.5}Cu_{0.5}Ga_yIn_{1-y}S_2$ for y = 0, 0.25, 0.5, 0.75, and 1.

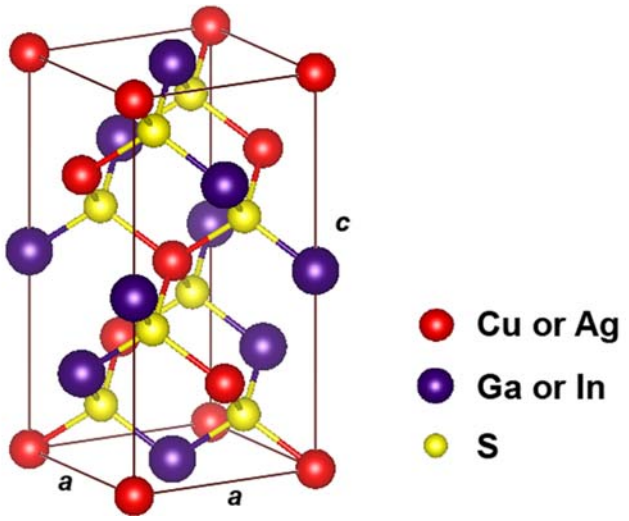

Figure 2. The chalcopyrite unit cell of CIGS\SIGS materials, labeled with lattice parameters *a* and *c*. The red spheres represent Ag and Cu, the purple spheres represent Ga and In, and the yellow spheres represent S.

Table 1 correlates changes in the observed lattice parameters and measured band gaps with stoichiometry in the quaternary system. Lattice parameters are plotted versus Ag and Ga fraction for both ternary and quaternary materials in Figure 3. With increasing Ga content, the lattice parameters *a* and *c* for the tetragonal unit cell decrease linearly, consistent with Vegard's Law. However, with increasing Ag content, the lattice parameter *a* increases linearly while the parameter *c* varies in a concave bowing fashion for all materials. A similar behavior of lattice parameters was reported by Matsushita *et al.* in the ternary $Ag_{1-x}Cu_xGaS_2$ system in 1993.[38] We hypothesize that this consistently observed behavior reflects the fact that the Cu and Ag may occupy slightly different positions within their S_4 coordination polyhedra in the mixed system, and further that the position offset may be more pronounced along the *c*-axis than in perpendicular directions, leading to a nonlinear variation of lattice parameter *c* but a linear change of parameter *a* versus the Ag to Cu ratio.

Table 1. Variation with composition of the Lattice Parameters *a* and *c* for the Tetragonal Unit Cell and the Band gap Eg for $Ag_xCu_{1-x}Ga_yIn_{1-y}S_2$

x	y	*a* (Å)[a]	*c* (Å) [a]	E_g (eV) [b]
0	1	5.360(2)	10.495(7)	2.34
0.2	1	5.414(5)	10.505(7)	2.28
0.5	1	5.531(6)	10.482(3)	2.21
1	1	5.765(5)	10.315(9)	2.50
0	0.5	5.442(6)	10.840(7)	1.74
0.9	0.5	5.776(8)	10.795(7)	1.78
0.2	0.25	5.546(2)	11.041(8)	1.52
0.5	0.25	5.648(5)	11.066(2)	1.56
0.5	0	5.685(5)	11.269(8)	1.37

[a] Lattice parameters were determined based on least squares fits to the powder XRD patterns by using the Topas diffraction suite. [b] Derived from UV-Vis diffuse reflectance spectroscopy by extrapolating the linear part of the $(\alpha h\upsilon)^2$ versus $h\upsilon$ based on the Equation (1) for direct-allowed transitions, which is discussed later in the paper.

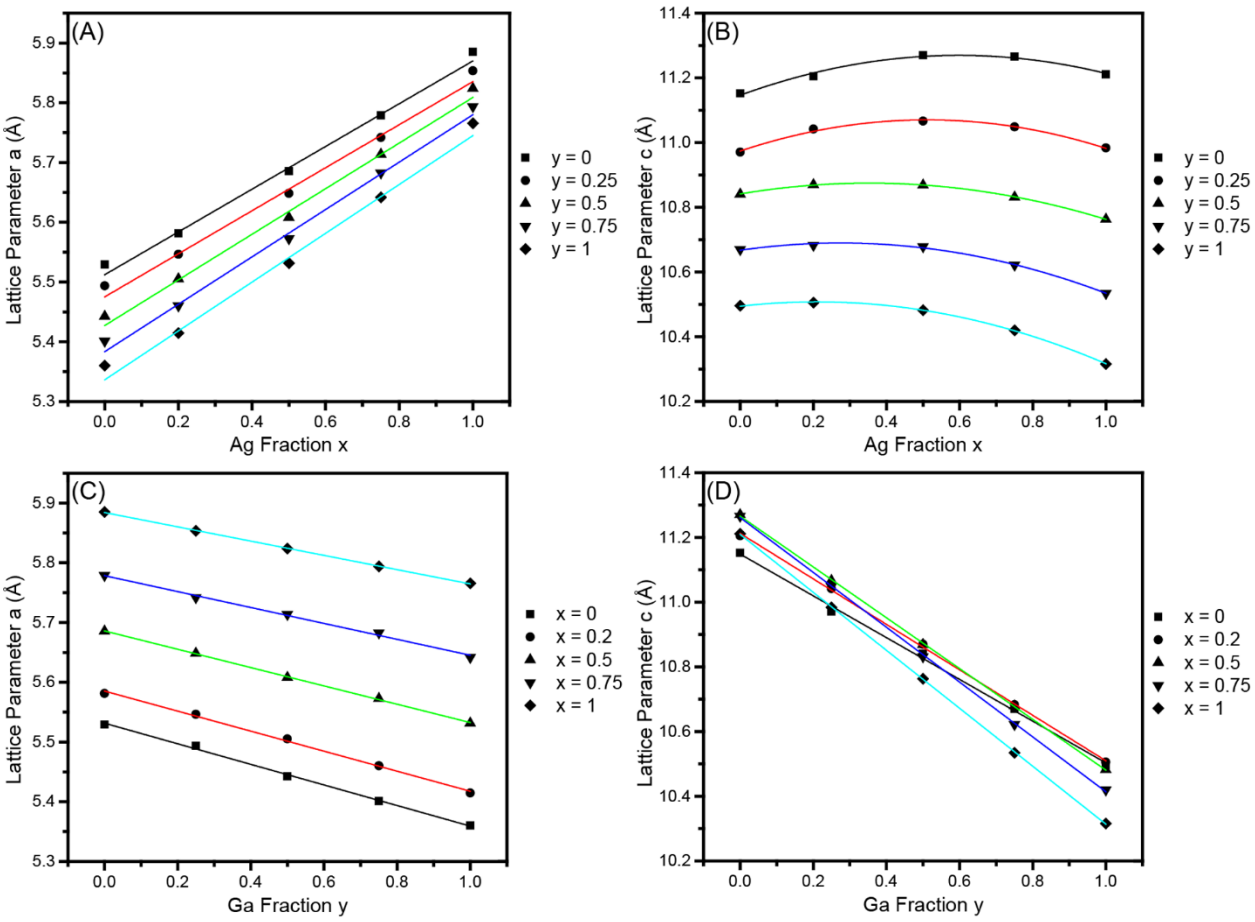

Figure 3. Correlation of tetragonal lattice parameters (*a* and *c*) with stoichiometry in the $Ag_xCu_{1-x}Ga_yIn_{1-y}S_2$ system. (A) Lattice parameter *a* versus mole fraction of silver, (B) Lattice parameter *c* versus mole fraction of silver, (C) Lattice parameter *a* versus mole fraction of gallium and (D) Lattice parameter *c* versus mole fraction of gallium.

Figure 4 shows representative SEM images of $Ag_xCu_{1-x}Ga_yIn_{1-y}S_2$ semiconductor powders. The EDX elemental analysis was consistent with the initial elemental ratios in the starting materials, confirming the chemical components of the samples and the successful formation of the solid solutions. EDX mapping data in Figure 4(C) and (D) confirm the uniform distribution of the elemental constituents in the solid solutions. In the microstructural images, the sample in Figure 4(A) shows nanostructured edges with well-defined steps while these features are absent in the

Figure 4(B) sample. It has been suggested by Jang *et al.* that such nanostructures may improve the absorbance of scattered incident photons and the migration of photogenerated electrons.[26] This is consistent with our observation in the photocatalytic water reduction experiments described below.

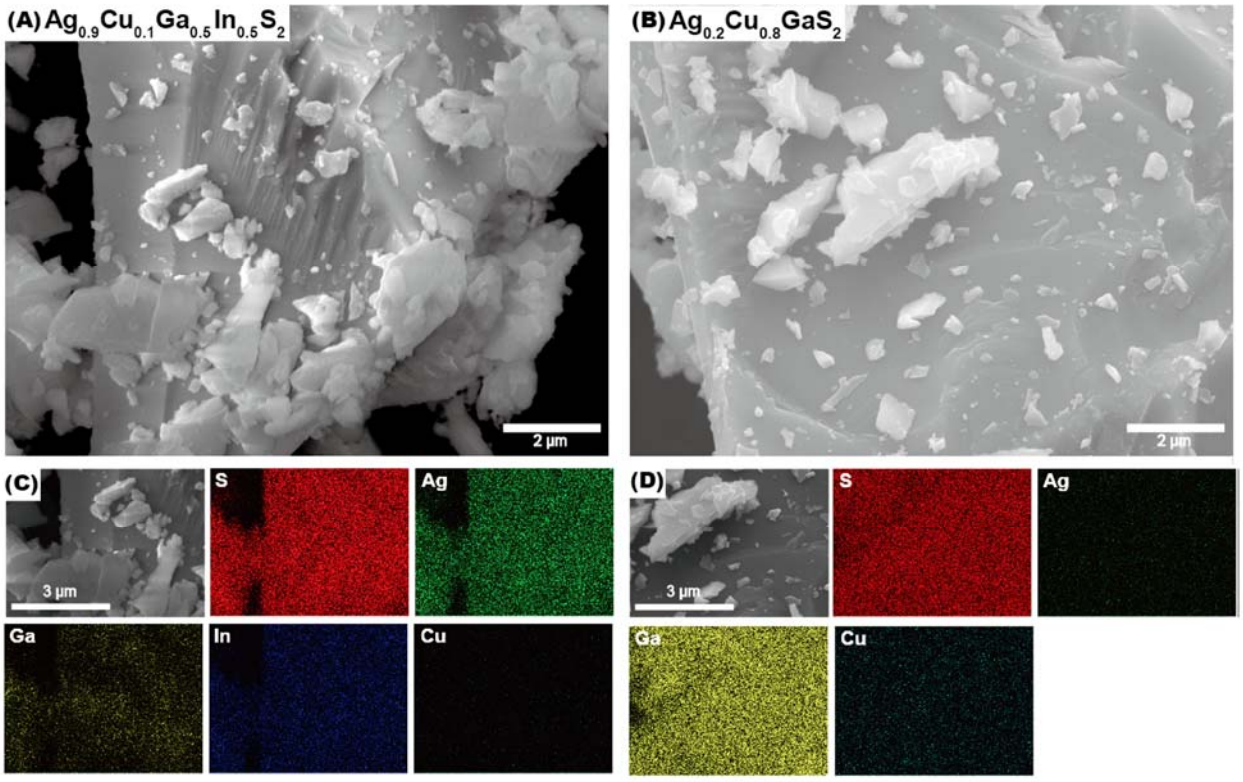

Figure 4. Representative scanning electron microscope images of $Ag_xCu_{1-x}Ga_yIn_{1-y}S_2$: (A) x = 0.9, y = 0.5, and (B) x = 0.2, y = 1, with the corresponding EDX mapping in (C) and (D) respectively. (The dark area of the mapping in (C) corresponds to the left corner area in the original SEM image, where there is a void in the material.)

Figure 5(A) shows the representative diffuse reflectance spectra of $Ag_{0.75}Cu_{0.25}Ga_yIn_{1-y}S_2$ ($0 \leqslant y \leqslant 1.0$) semiconductors. The spectra of other samples are shown in Figure S6-S10. Weak absorption tails were observed in the spectra of some samples, which are associated with

transitions from localized states in the band gap.[39] The band gap values were derived from UV-Vis diffuse reflectance spectroscopy by extrapolating the linear part of the $(\alpha h\upsilon)^2$ versus $h\upsilon$ based on the relation:

$$\alpha h\upsilon = A\,(h\upsilon - \mathrm{Eg})^{1/2} \quad (1)$$

for direct transitions, where A is a constant and α is the absorption coefficient (cm^{-1}).[34,40] They are visually represented in Figure 5(B)—clearly showing that band gap tuning is achieved by varying the Ag to Cu and Ga to In ratios. The band gap variation versus Ag fraction for samples where y is equal to 0.25 is consistent with the results published for $Ag_xCu_{1-x}Ga_{0.25}In_{0.75}S_2$ (x = 0, 0.1, 0.2, 0.3).[33] The variation in the band gap values is visible to the eye, as the color of $Ag_xCu_{1-x}Ga_yIn_{1-y}S_2$ powders change from dark green, to yellow, orange, red purple, and finally black (Figure S11).

While the change in band gap with the Ga:In ratio is relatively linear, as shown in Figure 5(B), an unexpected nonlinear variation of band gap values versus the Ag:Cu ratio is observed. This effect is most obvious when the IIIB site is totally populated with Ga, as seen in Figure 6 where the bandgap is observed to hit a minimum at a Ag:Cu = 0.7 generating a "V-shaped" plot. This variation is unexpected in that the structure of the compounds follows Vegard's rule, but the band gap behaves in a very not ideal manner in this respect. In all cases, the pure Ag-based ternaries have larger band gaps than the samples containing Cu. At a fixed Cu to Ag ratio in the quaternary solid solutions, the band gap shows either a monotonic increase or decrease with Ga to In ratio. The unusual properties of the Ag-only samples compared to those with a small amount of Cu present suggests that one of the band energies is dominated by Cu states.

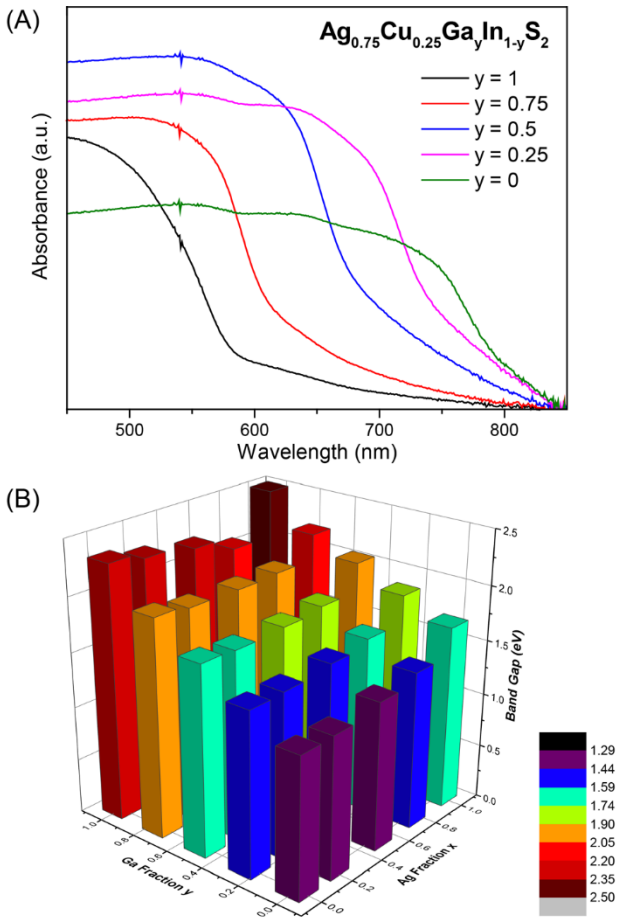

Figure 5. (A) Representative UV-vis absorbance spectra showing the effect of the Ga:In ratio in $Ag_{0.75}Cu_{0.25}Ga_yIn_{1-y}S_2$ on the optically observed band gap energy. The absorbance data were Kubelka-Munk transformed from reflectance raw data; (B) Optical band gap values of $Ag_xCu_{1-x}Ga_yIn_{1-y}S_2$ semiconductors versus chemical composition (both Ag:Cu ratio and Ga:In ratio) as derived from optical spectra. Band gap values are binned in 0.15 eV groups as shown by the colors.

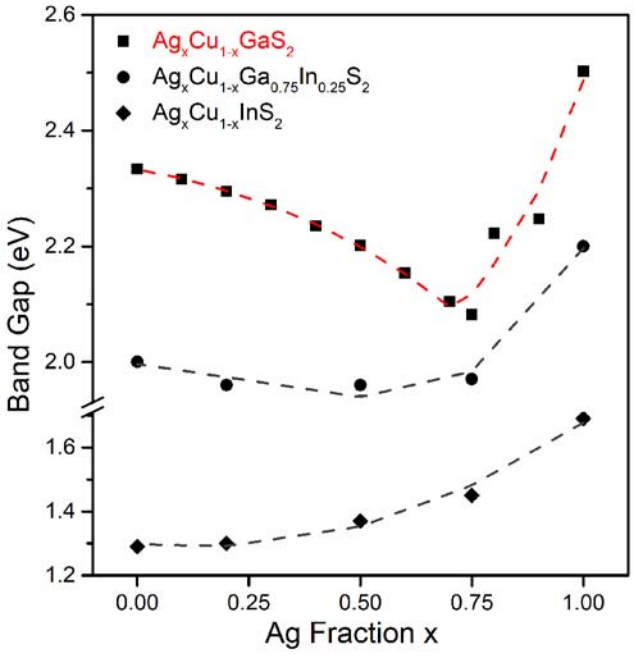

Figure 6. Band gap values of $Ag_xCu_{1-x}Ga_yIn_{1-y}S_2$ semiconductors (y = 0, 0.75 and 1) versus Ag:Cu ratio as derived from the optical spectra. A unique "V" shape was revealed on the band gap variation of $Ag_xCu_{1-x}GaS_2$.

In attempt to further understand the "V" shape of the band gap variation with no change in the average crystal structures, UPS experiments were carried out to estimate the position of the VBM for the $Ag_xCu_{1-x}GaS_2$ semiconductors (see Figure S12). As shown in Figure 7, the trend of band edge energies generally follows the "V" shape, suggesting a subtle second order electronic phase change around x = 0.7. The observation is currently under further study. Overall, we find that the $Ag_xCu_{1-x}Ga_yIn_{1-y}S_2$ semiconductor materials have band gaps ranging from 1.3 eV to 2.5 eV. As hypothesized, this is well-matched to the visible solar spectrum—supporting their potential applicability for photochemical water splitting.

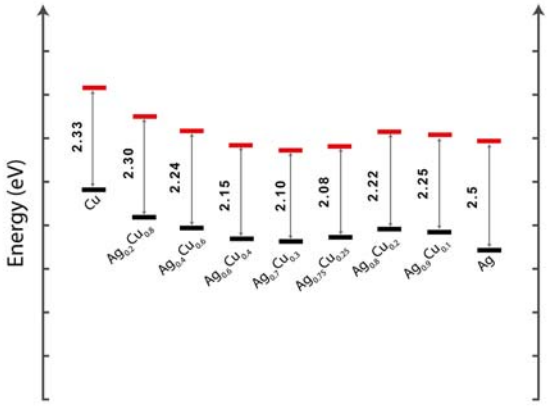

Figure 7. Band edge energies of $Ag_xCu_{1-x}GaS_2$ semiconductors versus Ag fraction, derived from UPS spectra along with band gap values from diffuse reflectance measurements.

Photochemical water reduction using ternary $Ag_xCu_{1-x}GaS_2$ ($0 \leqslant x \leqslant 1.0$) powders with sacrificial electron donors.

Table 2 shows varying reaction conditions of $Ag_xCu_{1-x}GaS_2$ solid solutions for photocatalytic H_2 evolution using sulfur-containing electron donors under near-UV (365 nm) light. For non-Pt-loaded tests over $Ag_xCu_{1-x}GaS_2$ solid solutions (x = 1, 0.9, 0.8, 0.6, 0.4, 0.2 and 0), all Cu-doping candidates possessed little activity under the experimental conditions employed. $AgGaS_2$, however, with a H_2 evolution rate of 0.08 $\mu molh^{-1}g^{-1}$, showed activity in the presence of Na_2SO_3 and Na_2S as sacrificial electron donors. Unfortunately, this material stopped producing H_2 after 4 h, suggesting photodegradation of the chalcopyrite. This conclusion was further supported by the observation of Ag_2S in a post-photolysis powder XRD pattern (Figure S13).

To optimize the activity of $Ag_xCu_{1-x}GaS_2$, a Pt-loading treatment (Table 2 entries 4, 6, and 7) was investigated for photocatalytic H_2 evolution. It has previously been noted in the $AgGaS_2$ system that a Pt co-catalyst serves as active sites for H_2 evolution, which not only facilitates H_2

production, but also increases the stability of $AgGaS_2$.[41] In the present experiments, Pt-deposition was confirmed by XPS and SEM analysis of the post-irradiated Pt-loaded $AgGaS_2$ (Figure S14). Addition of a platinum co-catalyst substantially increased the photocatalytic activity of $AgGaS_2$; further, the low activity Cu(I)-alloyed candidates were activated when platinum was introduced into the system. Interestingly, these activated candidates all lie on the right-hand branch of Figure 6, with high Ag-content, while the left-branch samples, which are richer in copper, didn't produce hydrogen even in the case of Pt deposition. This suggests that the nonlinear variation of photocatalytic properties may be related to the unique "V" shape of the Ag-content dependent band gap. In other words, the band gap variation induced by doping Cu in $AgGaS_2$ into the left branch of the "V" shape in Figure 6 appears to hinder the photocatalytic activity. We hypothesize that the conduction band edge potential might shift positive as the Cu concentration increases, which would thermodynamically hinder the hydrogen evolution of samples on the left-hand branch of the plot in Figure 6. However, this hypothesis is not consistent with the results of UPS measurements shown in Figure 7, as similar band edge positions were acquired for both an H_2-producing sample ($x = 0.8$) and a non-H_2-producing sample ($x = 0.4$). Another possible explanation of this observation is that Ag-rich samples may have more catalytically active surfaces than the Cu-rich ones. This intriguing phenomenon is still under study, and its origin may lay the foundation of the relationship between the photocatalytic behavior and the band structures of these materials.

From a practical point of view, the use of platinum as a cocatalyst is not ideal. In addition to questions of sustainability, the activity of a platinum photocatalyst might change depending on the exact composition of the electrolyte employed. Thus, we explored the addition of sacrificial donors (sulfite and sulfide) that could enhance hydrogen evolution in the absence of a platinum

catalyst.[5] The effects on the photocatalytic activity of $AgGaS_2$ obtained by varying sulfur-containing reagent are presented in entries 2, 3 5, 8 and 9 of Table 2. These results support the use of Na_2S as an electron donor, with a H_2 production rate of 0.94 $\mu molh^{-1}g^{-1}$, in the absence of a Pt catalyst, and a H_2 production rate of 4.77 $\mu molh^{-1}g^{-1}$, in the presence of platinum. The use of Na_2S as an optimized sacrificial electron donor was also supported by Meier *et al.* in 1984 with sulfides using for water reduction system.[43,44]

Table 2. Effects of Reaction and Preparation Condition on Photocatalytic H_2 evolution Activities of $Ag_xCu_{1-x}GaS_2$ (x = 1, 0.9, and 0.8)

Entry	Sample name	Reaction Condition[d]	Pt-co-catalyst loading/ wt%[c]	H_2 evolution rate ($\mu molh^{-1}g^{-1}$)
1	$AgGaS_2$	Na_2SO_3/ Na_2S[a]	none	0.08
2	$AgGaS_2$	Na_2SO_3[b]	none	0.25
3	$AgGaS_2$	Na_2S[b]	none	0.94
4	$AgGaS_2$	Na_2SO_3/ Na_2S[a]	0.5	1.25
5	$AgGaS_2$	Na_2S[b]	0.5	4.77
6	$Ag_{0.9}Cu_{0.1}GaS_2$	Na_2SO_3/ Na_2S[a]	0.5	0.59
7	$Ag_{0.8}Cu_{0.2}GaS_2$	Na_2SO_3/ Na_2S[a]	0.5	1.17
8	$Ag_{0.9}Cu_{0.1}GaS_2$	Na_2S[b]	0.5	4.65
9	$Ag_{0.8}Cu_{0.2}GaS_2$	Na_2S[b]	0.5	2.27

[a] A 15mL vial containing ca. 22 mg catalyst and 5 mL 0.25 M Na_2SO_3/0.35 M Na_2S solution; light source: 3 W 365 nm LED light; irradiation area, 2.3 cm^2. [b] 0.6 M of the electron donor was used. [c] The catalyst was treated with 0.5 wt% Pt loading by photodeposition of H_2PtCl_6 for 30 min, according to the literature method.[36,37] [d] The pH of all electrolytes employed was held constant at pH = 13.0 for all electrolyte combinations.

Photocatalytical water reduction with quaternary $Ag_xCu_{1-x}Ga_yIn_{1-y}S_2$ ($0 \leqslant x \leqslant 1.0$, $0 \leqslant y \leqslant 1.0$) powders.

Although improved performance of photocatalysis was observed by introducing a platinum co-catalyst, there is the concern that excess loading of the co-catalysts could decrease the system photocatalytic activity, due to active site blocking and unwanted charge recombination.[5] In addition to the aforementioned band gap narrowing by adding Cu into $AgInS_2$, co-addition of Ga and Cu has also been predicted to improve the efficiency of $AgInS_2$ by continuously shifting the band edge positions of both the VBM and CBM.[31,32] On the basis of these theoretical suggestions, the photocatalytic activities for H_2 evolution from (Ag,Cu)(Ga,In)S_2 are presented in Table 3. The ratio of Ga/In plays an essential role in improving the photocatalytic activity of Cu-doped $AgGaS_2$, which did not produce H_2 without the Pt co-catalyst in our tests. In particular, we note that $Ag_{0.75}Cu_{0.25}Ga_{0.25}In_{0.75}S_2$ demonstrates a catalytic performance comparable with that of Pt-loaded $Ag_xCu_{1-x}GaS_2$ (x = 1.0, 0.9 and 0.8) under the same experimental conditions (Table 2 entry 5, 8 and 9). A possible explanation for the improved activity is that the nanostructure features observed in Figure 4(A) may help incident photon absorption.[26,42]

Besides the obviously increased hydrogen evolution rate, $Ag_{0.9}Cu_{0.1}Ga_yIn_{1-y}S_2$ samples with relatively high hydrogen evolution rates were confirmed to continue producing H_2 after 72 hours of illumination. This suggests that greatly improved stability can be realized together with high efficiency for these quaternary semiconductors. The remarkable improvement of stability after adding a fourth cation into the system may be attributed to an inhibition in the quaternary system to the photodegradation of the semiconductors, mentioned in the previous section, as no obvious changes were detected between the pre- and post-photolysis quaternary semiconductor powders. Regarding practical application, the use of earth-abundant metals is more advantageous compared with noble-metal Pt. Therefore, the quaternary SCIGS semiconductors described here, with comparable water reduction efficiency and stability to the noble-metal-loaded ternaries as

shown in Figure 8, will be of value for further exploration as photoelectrode materials in photoelectrochemistry (PEC) systems.

Table 3. Photocatalytic Activities of $Ag_xCu_{1-x}Ga_yIn_{1-y}S_2$ (x = 0.9 and 0.75; y = 1, 0.8, 0.75, 0.5, 0.25 and 0.2)[a]

Entry	Sample name	H_2 evolution rate ($\mu molh^{-1}g^{-1}$)
1	$Ag_{0.9}Cu_{0.1}GaS_2$	0
2	$Ag_{0.9}Cu_{0.1}Ga_{0.8}In_{0.2}S_2$	1.43
3	$Ag_{0.9}Cu_{0.1}Ga_{0.5}In_{0.5}S_2$	1.49
4	$Ag_{0.9}Cu_{0.1}Ga_{0.2}In_{0.8}S_2$	1.20
5	$Ag_{0.75}Cu_{0.25}Ga_{0.75}In_{0.25}S_2$	2.90
6	$Ag_{0.75}Cu_{0.25}Ga_{0.5}In_{0.5}S_2$	2.24
7	$Ag_{0.75}Cu_{0.25}Ga_{0.25}In_{0.75}S_2$	3.15

[a] 0.6 M Na_2S solution was used, and other conditions are the same as Table 2.

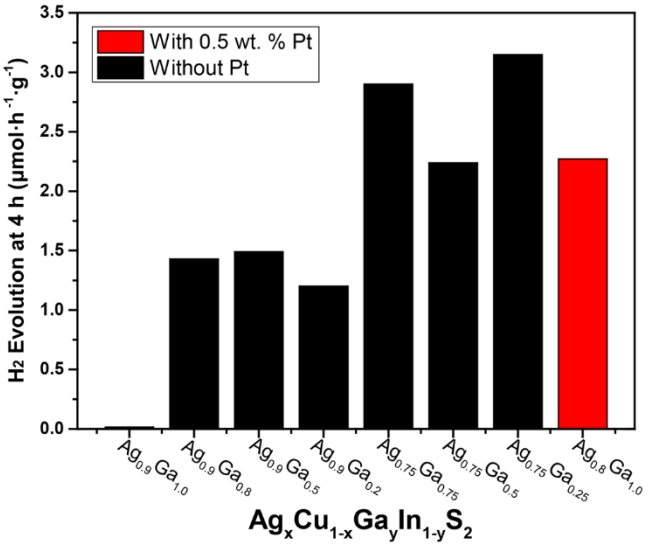

Figure 8. Hydrogen evolution rate at 4 h of quaternary $Ag_xCu_{1-x}Ga_yIn_{1-y}S_2$ (x = 0.9 and 0.75; y = 0.8, 0.75, 0.5 0.25 and 0.2) together with ternary $Ag_{0.9}Cu_{0.1}GaS_2$ and $Ag_{0.8}Cu_{0.2}GaS_2$ for comparison. 0.6 M Na_2S solution was used, other conditions are the same as Table 2.

CONCLUSIONS

Quaternary $Ag_xCu_{1-x}Ga_yIn_{1-y}S_2$ ($0 \leqslant x \leqslant 1.0$ and $0 \leqslant y \leqslant 1.0$) semiconductor bulk materials have been prepared by the solid-state reaction method and their properties relevant to their use as water-spitting electrodes are reported for the first time. XRD spectra confirmed the formation of the chalcopyrite structure and SEM was employed to characterize the surface morphologies of the materials. Both the VBM and CBM were variable in the solid solution, and the values of band gap, measured by diffuse reflectance spectroscopy, were found to range from 1.3 to 2.5 eV. A unique "V" shape was revealed in the band gap variation of $Ag_xCu_{1-x}GaS_2$ and the quaternary systems versus Ag fraction, which appears to be empirically related to their unexpected nonlinear behaviors in hydrogen evolution. Photocatalytic water reduction experiments were carried out on the materials in powder form with sacrificial electron donors, revealing that the quaternary semiconductor with composition near $Ag_{0.75}Cu_{0.25}Ga_{0.25}In_{0.75}S_2$ is able to reach, without noble-meta-loading, comparable performance to noble-metal-loaded ternary chalcopyrites. This quaternary material displays relatively high efficiency and high stability compared with the frequently studied ternary end members (i.e. $x = 0$ or $y = 0$) of the $Ag_xCu_{1-x}Ga_yIn_{1-y}S_2$ system, indicative of the potential of the quaternary system for PEC applications. Further study of the band structures and photocatalytic behavior of the SCIGS family, with the goal of understanding the relationship between these two properties is underway in our laboratories. However, at this point the correlation of bulk electronic structure with photocatalytic activity provides a new aspect of the semiconductor-electrolyte interface, which can be used to design improved water splitting photoactive interfaces.

ASSOCIATED CONTENT

Supporting Information. Supporting information is provided as a supplement to the main text. The XRD patterns and UV-vis absorbance spectra of prepared semiconductors that are not included in the main text are shown, as are a photograph to show the color change of the samples, the UPS spectra, the XRD pattern comparison of a sample pre- and post-photolysis, and the XPS and SEM analysis of the Pt-loaded sample.

AUTHOR INFORMATION

Corresponding Author

*E-mail: rcava@princeton.edu

*E-mail: bocarsly@princeton.edu

ORCID

Andrew B. Bocarsly: 0000-0003-3718-0933

Author Contributions

The manuscript was written through contributions of all authors. All authors have given approval to the final version of the manuscript.

Notes

The authors declare no competing financial interest.

ACKNOWLEDGMENT

The authors acknowledge support of this research funding from the Office of Basic Energy Sciences, Department of Energy. The solid state synthesis and material characterization were

performed under the direction of R.J.C. (Grant DE-FG02-98ER45706). Photochemical experiments were performed under the direction of A.B.B. (Grant DE-SC0002133). We would also like to thank John Schreiber and Nan Yao for assistance with scanning electron microscopy, Yao-Wen Yeh for assistance with UPS measurements, and Gregory D. Scholes for assistance with diffuse reflectance spectroscopy.

REFERENCES

(1) Fujishima, A.; Honda, K. Electrochemical Photolysis of Water at a Semiconductor Electrode. *Nature*. **1972,** *238*, 37–38.

(2) Kudo, A.; Miseki, Y. Heterogeneous photocatalyst materials for water splitting. *Chem. Soc. Rev.* **2009,** *38*, 253–278.

(3) Xing, C.; Zhang, Y.; Yan, W.; Guo, L. Band structure-controlled solid solution of $Cd_{1-x}Zn_xS$ photocatalyst for hydrogen production by water splitting. *Int. J. Hydrog. Energy*. **2006,** *31*, 2018–2024.

(4) Maeda, K.; Domen, K. Photocatalytic Water Splitting: Recent Progress and Future Challenges. *J. Phys. Chem. Lett.* **2010,** *1*, 2655–2661.

(5) Ran, J.; Zhang, J.; Yu, J.; Jaroniec, M.; Zhang, Q. S. Earth-abundant cocatalysts for semiconductor-based photocatalytic water splitting. *Chem. Soc. Rev.* **2014,** *43*, 7787–7812.

(6) Navarro Yerga, R. M.; Álvarez Galván, M. C.; del Valle F., Villoria de la Mano, J. A.; Fierro, J. L. G. Water Splitting on Semiconductor Catalysts under Visible-Light Irradiation. *ChemSusChem*. **2009,** *2*, 471-485.

(7) Wolcott, A.; Smith, W. A.; Kuykendall, T. R.; Zhao, Y.; Zhang, J. Z. Photoelectrochemical Study of Nanostructured ZnO Thin Films for Hydrogen Generation from Water Splitting. *Adv. Funct. Mater.* **2009,** *19*, 1849–1856.

(8) Yang, X.; Wolcott, A.; Wang, G.; Sobo, A.; Fitzmorris, R. C.; Qian, F.; Zhang, J. Z.; Li, Y. Nitrogen-Doped ZnO Nanowire Arrays for Photoelectrochemical Water Splitting. *Nano Lett.* **2009,** *9*, 2331–2336.

(9) Lin, Y.-G.; Hsu, Y.-K.; Chen, Y.-C.; Chen, L.-C.; Chen, S.-Y.; Chen, K.-H. Visible-light-driven photocatalytic carbon-doped porous ZnO nanoarchitectures for solar water-splitting. *Nanoscale.* **2012,** *4*, 6515–6519.

(10) Sayama, K.; Nomura, A.; Arai, T.; Sugita, T.; Abe, R.; Yanagida, M.; Oi, T.; Iwasaki, Y.; Abe, Y.; Sugihara, H. Photoelectrochemical Decomposition of Water into H_2 and O_2 on Porous $BiVO_4$ Thin-Film Electrodes under Visible Light and Significant Effect of Ag Ion Treatment. *J. Phys. Chem. B*. **2006,** *110*, 11352–11360.

(11) Ye, H.; Lee, J.; Jang, J. S.; Bard, A. J. Rapid Screening of $BiVO_4$-Based Photocatalysts by Scanning Electrochemical Microscopy (SECM) and Studies of Their Photoelectrochemical Properties. *J. Phys. Chem. C*. **2010,** *114*, 13322–13328.

(12) Iwase, A.; Kudo, A. Photoelectrochemical water splitting using visible-light-responsive $BiVO_4$ fine particles prepared in an aqueous acetic acid solution. *J. Mater. Chem.* **2010,** *20*, 7536–7542.

(13) Kim, T. W.; Choi, K.-S. Nanoporous $BiVO_4$ Photoanodes with Dual-Layer Oxygen Evolution Catalysts for Solar Water Splitting. *Science.* **2014,** 1245026.

(14) Abdi, F. F.; Han, L.; Smets, A. H. M.; Zeman, M.; Dam, B.; van de Krol, R. Efficient solar water splitting by enhanced charge separation in a bismuth vanadate-silicon tandem photoelectrode. *Nat. Commun.* **2013,** *4*, 2195-2201.

(15) Hwang, D. W.; Kim, J.; Park, T. J.; Lee, J. S. Mg-Doped WO_3 as a Novel Photocatalyst for Visible Light-Induced Water Splitting. *Catal. Lett.* **2002,** *80*, 53–57.

(16) Miller, E. L.; Marsen, B.; Cole, B.; Lum, M. Low-Temperature Reactively Sputtered Tungsten Oxide Films for Solar-Powered Water Splitting Applications. *Electrochem. Solid-State Lett.* **2006,** *9*, G248–G250.

(17) Hong, S. J.; Jun, H.; Borse, P. H.; Lee, J. S. Size effects of WO_3 nanocrystals for photooxidation of water in particulate suspension and photoelectrochemical film systems. *Int. J. Hydrog. Energy.* **2009,** *34*, 3234–3242.

(18) Arriaga, L. G.; Fernández, A. M.; Solorza, O. Preparation and characterization of (Zn,Cd)S photoelectrodes for hydrogen production. *Int. J. Hydrog. Energy.* **1998,** *23*, 995–998.

(19) Zhang, J.; Wang, L.; Liu, X.; Li, X.; Huang, W. High-performance CdS–ZnS core–shell nanorod array photoelectrode for photoelectrochemical hydrogen generation. *J. Mater. Chem. A*. **2015,** *3*, 535–541.

(20) Abe, R.; Higashi, M.; Domen, K. Facile Fabrication of an Efficient Oxynitride TaON Photoanode for Overall Water Splitting into H_2 and O_2 under Visible Light Irradiation. *J. Am. Chem. Soc.* **2010,** *132*, 11828–11829.

(21) Park, J. E.; Hu, Y.; Krizan, J. W.; Gibson, Q. D.; Tayvah, U. T.; Selloni, A.; Cava, R. J.; Bocarsly, A. B. Stable Hydrogen Evolution from an $AgRhO_2$ Photocathode under Visible Light. *Chem. Mater.* **2018,** *30*, 2574-2582.

(22) Gu, J.; Yan, Y.; Krizan, J. W.; Gibson, Q. D.; Detweiler, Z. M.; Cava, R. J.; Bocarsly, A. B. p-Type $CuRhO_2$ as a Self-Healing Photoelectrode for Water Reduction under Visible Light. *J. Am. Chem. Soc.* **2014,** *136*, 830–833.

(23) Maeda, K. Photocatalytic water splitting using semiconductor particles: History and recent developments. *J. Photochem. Photobiol. C Photochem. Rev.* **2011,** *12*, 237–268.

(24) Kudo, A. Development of photocatalyst materials for water splitting. *Int. J. Hydrog. Energy.* **2006,** *31*, 197–202.

(25) Tsuji, I.; Kato, H.; Kobayashi, H.; Kudo, A. Photocatalytic H_2 Evolution under Visible-Light Irradiation over Band-Structure-Controlled $(CuIn)_xZn_{2(1-x)}S_2$ Solid Solutions. *J. Phys. Chem. B*. **2005,** *109*, 7323–7329.

(26) Jang, J. S.; Borse, P. H.; Lee, J. S.; Choi, S. H.; Kim, H. G. Indium induced band gap tailoring in $AgGa_{1-x}In_xS_2$ chalcopyrite structure for visible light photocatalysis. *J. Chem. Phys.* **2008,** *128*, 154717.

(27) Kaga, H.; Tsutsui, Y.; Nagane, A.; Iwase, A.; Kudo, A. An effect of Ag(I)-substitution at Cu sites in $CuGaS_2$ on photocatalytic and photoelectrochemical properties for solar hydrogen evolution. *J. Mater. Chem. A*. **2015,** *3*, 21815–21823.

(28) Luo, J.; Tilley, S. D.; Steier, L.; Schreier, M.; Mayer, M. T.; Fan, H. J.; Grätzel, M. Solution Transformation of Cu_2O into $CuInS_2$ for Solar Water Splitting. *Nano Lett.* **2015,** *15*, 1395–1402.

(29) Zhang, L.; Minegishi, T.; Nakabayashi, M.; Suzuki, Y.; Seki, K.; Shibata, N.; Kubota, J.; Domen, K. Durable hydrogen evolution from water driven by sunlight using (Ag,Cu)$GaSe_2$ photocathodes modified with CdS and $CuGa_3Se_5$. *Chem. Sci.* **2015,** *6*, 894–901.

(30) Stanbery, B. J. Copper Indium Selenides and Related Materials for Photovoltaic Devices. *Crit. Rev. Solid State Mater. Sci.* **2002,** *27*, 73–117.

(31) Huang, D.; Ju, Z.; Ning, H.; Li, C.; Yao, C.; Guo, J. First-principles study on $CuAlTe_2$ and $AgAlTe_2$ for water splitting. *Mater. Chem. Phys.* **2014,** *148*, 882–886.

(32) Huang, D.; Persson, C. Photocatalyst $AgInS_2$ for active overall water-splitting: A first-principles study. *Chem. Phys. Lett.* **2014,** *591*, 189–192.

(33) Septina, W.; Sugimoto, M.; Chao, D.; Shen, Q.; Nakatsuka, S.; Nose, Y.; Harada, T.; Ikeda, S. Photoelectrochemical Water Reduction over Wide Gap (Ag,Cu)(In,Ga)S_2 Thin Film Photocathodes. *Phys. Chem. Chem. Phys.* **2017**, *19*, 12502–12508.

(34) Tarasova, A. Y.; Isaenko, L. I.; Kesler, V. G.; Pashkov, V. M.; Yelisseyev, A. P.; Denysyuk, N. M.; Khyzhun, O. Y. Electronic structure and fundamental absorption edges of KPb_2Br_5, $K_{0.5}Rb_{0.5}Pb_2Br_5$, and $RbPb_2Br_5$ single crystals. *J. Phys. Chem. Solids*. **2012,** *73*, 674–682.

(35) Tinker, L. L.; McDaniel, N. D.; Curtin, P. N.; Smith, C. K.; Ireland, M. J.; Bernhard, S. Visible Light Induced Catalytic Water Reduction without an Electron Relay. *Chemistry – A European Journal.* **2007,** *13*, 8726–8732.

(36) Kraeutler, B.; Bard, A. J. Heterogeneous Photocatalytic Preparation of Supported Catalysts. Photodeposition of Platinum on Titanium Dioxide Powder and Other Substrates. *J. Am. Chem. Soc.* **1978**, *100*, 4317–4318.

(37) Lin, P.-C.; Wang, P.-Y.; Li, Y.-Y.; Hua, C. C.; Lee, T.-C. Enhanced photocatalytic hydrogen production over In-rich (Ag–In–Zn)S particles. *Int. J. Hydrog. Energy*. **2013,** *38*, 8254–8262.

(38) Matsushita, H.; Endo, S.; Irie, T. Structural and Optical Properties of the $Cu_{1-x}Ag_xGaS_2$ System. *Jpn. J. Appl. Phys.* **1993,** *32*, L1049.

(39) Wood, D. L.; Tauc, J. Weak Absorption Tails in Amorphous Semiconductors. *Phys. Rev. B*. **1972,** *5*, 3144–3151.

(40) Chavhan, S.; Sharma, R. Growth, structural and optical properties of non-stoichiometric $CuIn(S_{1-x}Se_x)_2$ thin films deposited by solution growth technique for photovoltaic application. *J. Phys. Chem. Solids*. **2006,** *67*, 767–773.

(41) Tsuji, I.; Kato, H.; Kobayashi, H.; Kudo, A. Photocatalytic H_2 Evolution Reaction from Aqueous Solutions over Band Structure-Controlled $(AgIn)_xZn_{2(1-x)}S_2$ Solid Solution Photocatalysts with Visible-Light Response and Their Surface Nanostructures. *J. Am. Chem. Soc.* **2004,** *126*, 13406–13413.

(42) Chen, S.; Gong, X. G.; Wei, S.-H. Band-structure anomalies of the chalcopyrite semiconductors $CuGaX_2$ versus $AgGaX_2$ (X = S and Se) and their alloys. *Phys. Rev. B*. **2007,** *75*, 205209.

(43) Buehler, N.; Meier, K.; Reber, J. F. Photochemical hydrogen production with cadmium sulfide suspensions. *J. Phys. Chem.* **1984,** *88*, 3261–3268.

(44) Reber, J. F.; Meier, K. Photochemical production of hydrogen with zinc sulfide suspensions. *J. Phys. Chem.* **1984,** *88*, 5903–5913.

TOC Graphic

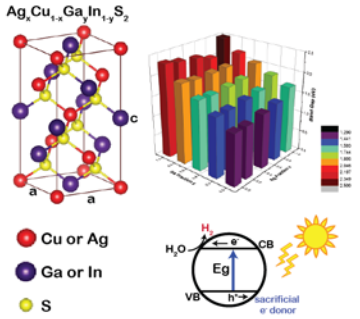
Ag$_x$Cu$_{1-x}$Ga$_y$In$_{1-y}$S$_2$
c
a
a
Cu or Ag
Ga or In
S
H$_2$
H$_2$O
e$^-$
CB
Eg
VB
h$^+$
sacrificial
e$^-$ donor